ADAPTIVE SPARSE GALERKIN METHODS FOR VIBRATING CONTINUOUS STRUCTURES

Zaid Ahsan[1], Thomas K. Uchida[2] and C.P. Vyasarayani[1]
[1]*Department of Mechanical and Aerospace Engineering, Indian Institute of Technology Hyderabad, Telangana, India*
[2]*Department of Bioengineering, Stanford University, Stanford, CA, U.S.A.*
E-mail: tkuchida@stanford.edu

Received March 2015, Accepted May 2015
No. 15-CSME-06, E.I.C. Accession Number 3781

ABSTRACT
Adaptive reduced-order methods are explored for simulating continuous vibrating structures. The Galerkin method is used to convert the governing partial differential equation (PDE) into a finite-dimensional system of ordinary differential equations (ODEs) whose solution approximates that of the original PDE. Sparse projections of the approximate ODE solution are then found at each integration time step by applying either the least absolute shrinkage and selection operator (lasso) or the optimal subset selection method. We apply the two projection schemes to the simulation of a vibrating Euler–Bernoulli beam subjected to nonlinear unilateral and bilateral spring forces. The subset selection approach is found to be superior for this application, as it generates a solution with similar sparsity but substantially lower error than the lasso.

Keywords: Galerkin; lasso; reduction; shrinkage; sparse; subset selection.

MÉTHODE ADAPTIVE DE DISPERSION DE TYPE GALERKIN POUR DES STRUCTURES CONTINUELLES EN ÉTAT DE VIBRATION

RÉSUMÉ
Des méthodes adaptives d'ordre réduit sont étudiées pour la simulation de structures continuelles en état de vibration. La méthode Galerkin est utilisée pour convertir les équations différentielles partielles (EDP) gouvernantes en un système dimensionnel fini d'équations différentielles ordinaires (EDO), dont la solution s'approche de l'original EDP. Des projections dispersées de la solution EDO approximative sont ensuite trouvées pour chaque intégration de la variable temps en appliquant soit la plus petite valeur absolue de retrait de sélection (lasso) ou la méthode du sous-ensemble optimal. Nous appliquons les deux schémas de projection à la simulation d'une poutre vibrante Euler–Bernoulli soumise à des tensions de ressort nonlinéaires unilatérales et bilatérales. L'approche de sélection du sous-ensemble s'est révélée supérieure pour cette application, parce qu'elle génère une solution similaire de dispersion, mais avec un taux d'erreurs de dispersion considérablement plus faible que le lasso.

Mots-clés : Galerkin; lasso; réduction; retrait; dispersion; sélection du sous-ensemble.

1. INTRODUCTION

The governing dynamics of vibrating continuous structures are described by partial differential equations (PDEs) [1]. Several methods have been developed for solving these time-dependent PDEs, including finite difference [2], finite element [3], and pseudo-spectral collocation [4] approaches. Spectral methods (e.g., the Galerkin method) involve approximating the solution using global shape functions that span the entire domain of the solution, resulting in a system of ordinary differential equations (ODEs). If the solution of the PDE is smooth, the solution obtained using a spectral method will converge to the exact solution exponentially as the number of terms in the approximation is increased [4]. Thus, spectral methods naturally lead to fewer time-dependent ODEs than finite difference or finite element approaches; however, it is often unclear how many terms should be retained in the series solution, particularly when studying nonlinear systems. A typical approach is to truncate the series solution using a heuristic based on the frequency content of the external forces or the frequencies of interest in the solution. As might be expected, such heuristics perform poorly in systems with strong intermodal coupling or when subjected to external forces of unanticipated frequencies.

At every instant in time, the solution of the PDEs (e.g., the displacement of a vibrating structure) can be treated as a signal in space. The theory of compressive sensing informs us that a signal can be reconstructed using a sparse set of coefficients [5]. The present study is inspired by this theory as well as the work of Schaeffer et al. [6], who use soft thresholding to obtain sparsity in their solutions of multiscale systems (first-order PDEs in time). In this work, we develop an adaptive reduced-order method for simulating continuous vibrating structures (second-order PDEs in time), and compare the least absolute shrinkage and selection operator (lasso) with the optimal subset selection method [7]. We first discretize the governing PDE to obtain a finite-dimensional system of ODEs whose solution approximates that of the original PDE. One of two optimization strategies is then employed to seek the most informative sparse solution at each integration time step. In the first case, we apply the lasso at each time step to reduce the number of nonzero coefficients in the approximate series solution. Since the resulting optimization problem has a closed-form solution, the reduction step can be performed with minimal computational expense. In the second case, we apply the optimal subset selection method. We demonstrate the developed approach using a forced vibration problem containing nonlinear modal interactions, and compare the results obtained using the lasso and optimal subset selection strategies.

Several techniques have been developed for reducing models to their most essential components, most of which apply only to linear or linearized systems [8, 9]. A well-known strategy for nonlinear systems is the proper orthogonal decomposition (POD) or principal component analysis [10, 11], and is related to the sparse approaches explored herein. The POD technique uses a linear transformation to project the original n-dimensional solution space into a k-dimensional space, $k < n$, where each coordinate direction k_j is the jth most informative and is orthogonal to the first $j-1$ coordinate directions. This transformation can be used to project a dynamical system into a space of lower dimensionality while retaining as much information about its behavior as possible. The transformation matrix is computed by performing a partial eigendecomposition of the mean-adjusted matrix of state vector snapshots. Therein lies the key difference between the POD technique and the approaches explored in this work: the former employs a transformation matrix, which will likely need to be recomputed periodically for highly nonlinear systems; the lasso and subset selection methods require no information from past states.

The mathematical model for the developed approach is discussed in Section 2, where we describe the theory in the context of a simply supported beam subjected to forces exerted by nonlinear unilateral and bilateral springs. Note that this concrete example is used only for demonstration purposes; the theory is equally applicable to any vibrating structure whose solution is approximated using a spectral method. Sev-

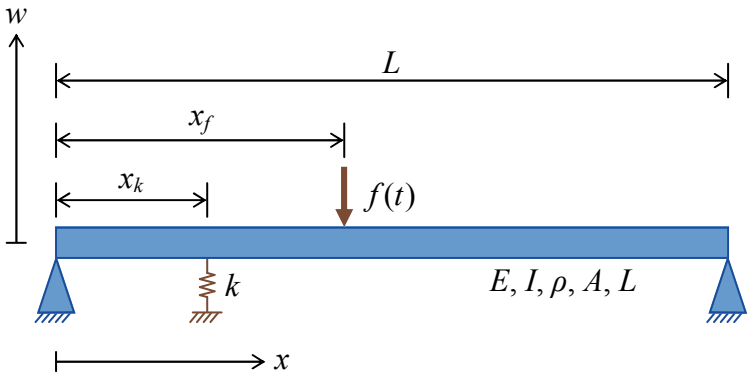

Fig. 1. Simply supported beam of length L subjected to a nonlinear force $f(t)$ at $x = x_f$ and a nonlinear unilateral or bilateral spring force at $x = x_k$. Displacements $w(x,t)$ are obtained using classical and sparse Galerkin methods.

eral numerical test cases are presented in Section 3 to compare the efficacy of the lasso and subset selection strategies. Conclusions are provided in Section 4.

2. MATHEMATICAL MODELING

To demonstrate the adaptive reduced-order modeling approach, we consider a vibrating simply supported beam subjected to nonlinear unilateral and bilateral spring forces [12], as shown in Fig. 1. Using Euler–Bernoulli beam theory [1] and assuming small deflections $w(x,t)$, the dynamics of the beam are governed by a single PDE:

$$EI\frac{\partial^4 w}{\partial x^4} + \rho A\frac{\partial^2 w}{\partial t^2} = f(t)\,\delta(x - x_f) - kw(x_k,t)^3\,\delta(x - x_k) \tag{1}$$

where flexural rigidity is the product of Young's modulus E and area moment of inertia I, linear mass density is the product of density ρ and cross-sectional area A, an external force $f(t)$ is applied at $x = x_f$, and a nonlinear spring of stiffness k is located at $x = x_k$. Under the assumption that the beam is simply supported, we have the following boundary conditions:

$$w(0,t) = 0, \quad \frac{\partial^2 w(0,t)}{\partial x^2} = 0 \tag{2a}$$

$$w(L,t) = 0, \quad \frac{\partial^2 w(L,t)}{\partial x^2} = 0 \tag{2b}$$

where L is the length of the beam. The initial conditions are defined as follows:

$$w(x,0) = \psi(x), \quad \frac{\partial w(x,0)}{\partial t} = \varphi(x) \tag{3}$$

where $\psi(x)$ and $\varphi(x)$ are arbitrary functions defined over the domain $x \in [0,L]$. When the spring is acting unilaterally, it exerts force only when the beam has deflected in the negative direction at the location of the spring, which we model by replacing k with k_u:

$$k_\mathrm{u} = \begin{cases} k, & \text{if } w(x_k,t) < 0 \\ 0, & \text{otherwise} \end{cases} \tag{4}$$

We now introduce the following parameters into Eqs. (1), (2), and (3):

$$\tilde{x} = \frac{x}{L}, \quad \tilde{w} = \frac{w}{L}, \quad \tilde{t} = t\sqrt{\frac{EI}{\rho AL^4}}, \quad \tilde{f} = \frac{fL^3}{EI}, \quad \tilde{k} = \frac{kL^6}{EI} \tag{5}$$

Upon substituting Eq. (5) into Eqs. (1), (2), and (3), we obtain the following nondimensional initial–boundary value problem:

$$\frac{\partial^4 w}{\partial x^4} + \frac{\partial^2 w}{\partial t^2} = f(t)\,\delta(x-x_f) - kw(x_k,t)^3\,\delta(x-x_k) \tag{6}$$

$$w(0,t) = 0, \quad \frac{\partial^2 w(0,t)}{\partial x^2} = 0 \tag{7a}$$

$$w(1,t) = 0, \quad \frac{\partial^2 w(1,t)}{\partial x^2} = 0 \tag{7b}$$

$$w(x,0) = \psi(x), \quad \frac{\partial w(x,0)}{\partial t} = \varphi(x) \tag{8}$$

where we have dropped the tilde for notational convenience.

We assume the following series solution to Eq. (6):

$$w(x,t) = \boldsymbol{\phi}(x)^{\mathrm{T}}\boldsymbol{\eta}(t) \tag{9}$$

where $\boldsymbol{\phi}(x) = [\sin(\pi x), \sin(2\pi x), \ldots, \sin(N\pi x)]^{\mathrm{T}}$ are the N basis functions retained in the series solution and $\boldsymbol{\eta}(t) = [\eta_1(t), \eta_2(t), \ldots, \eta_N(t)]^{\mathrm{T}}$ are the time-dependent coordinates. Note that the assumed solution (Eq. (9)) satisfies the boundary conditions (Eq. (7)) at all time by construction. Upon substituting the series solution (Eq. (9)) into Eq. (6), we obtain the following:

$$\boldsymbol{\phi}^{\mathrm{IV}}(x)^{\mathrm{T}}\boldsymbol{\eta}(t) + \boldsymbol{\phi}(x)^{\mathrm{T}}\ddot{\boldsymbol{\eta}}(t) = f(t)\,\delta(x-x_f) - kw(x_k,t)^3\,\delta(x-x_k) \tag{10}$$

where $\boldsymbol{\phi}^{\mathrm{IV}}(x) \triangleq \partial^4\boldsymbol{\phi}(x)/\partial x^4$. Applying the Galerkin method, we multiply Eq. (10) by $\boldsymbol{\phi}(x)$ and integrate over the domain, obtaining the following ODEs in time:

$$\begin{aligned}&\int_0^1 \boldsymbol{\phi}(x)\boldsymbol{\phi}^{\mathrm{IV}}(x)^{\mathrm{T}}dx\,\boldsymbol{\eta}(t) + \int_0^1 \boldsymbol{\phi}(x)\boldsymbol{\phi}(x)^{\mathrm{T}}dx\,\ddot{\boldsymbol{\eta}}(t)\\ &\approx f(t)\int_0^1 \delta(x-x_f)\,\boldsymbol{\phi}(x)\,dx - k\left(\boldsymbol{\phi}(x_k)^{\mathrm{T}}\boldsymbol{\eta}(t)\right)^3\int_0^1 \delta(x-x_k)\,\boldsymbol{\phi}(x)\,dx\end{aligned} \tag{11}$$

We define mass and stiffness matrices $\mathbf{M}$ and $\mathbf{K}$ as follows:

$$\mathbf{M} \triangleq \int_0^1 \boldsymbol{\phi}(x)\boldsymbol{\phi}(x)^{\mathrm{T}}dx, \quad \mathbf{K} \triangleq \int_0^1 \boldsymbol{\phi}(x)\boldsymbol{\phi}^{\mathrm{IV}}(x)^{\mathrm{T}}dx \tag{12}$$

and recall the following property of the Dirac delta function:

$$\int_0^1 \delta(x-\zeta)\,\boldsymbol{\phi}(x)\,dx = \boldsymbol{\phi}(\zeta) \tag{13}$$

whereupon we obtain a simplified expression of the system ODEs (Eq. (11)):

$$\mathbf{M}\ddot{\boldsymbol{\eta}}(t) + \mathbf{K}\boldsymbol{\eta}(t) = f(t)\,\boldsymbol{\phi}(x_f) - k\left(\boldsymbol{\phi}(x_k)^{\mathrm{T}}\boldsymbol{\eta}(t)\right)^3\boldsymbol{\phi}(x_k) \tag{14}$$

To include the effects of energy dissipation, a Rayleigh damping [1] term with coefficients α and β is introduced into the undamped beam model (Eq. (14)):

$$\mathbf{M}\ddot{\eta}(t)+\mathbf{C}\dot{\eta}(t)+\mathbf{K}\eta(t)=f(t)\,\phi(x_f)-k\left(\phi(x_k)^{\mathrm{T}}\eta(t)\right)^3\phi(x_k) \tag{15}$$

where $\mathbf{C}\triangleq\alpha\mathbf{M}+\beta\mathbf{K}$. To obtain initial conditions $\eta(0)$ and $\dot{\eta}(0)$, we first substitute the solution (Eq. (9)) into the initial conditions (Eq. (8)):

$$\phi(x)^{\mathrm{T}}\eta(0)=\psi(x) \tag{16a}$$

$$\phi(x)^{\mathrm{T}}\dot{\eta}(0)=\varphi(x) \tag{16b}$$

Upon pre-multiplying by $\phi(x)$ and integrating over the domain, we obtain the following initial conditions for Eq. (15):

$$\eta(0)=\mathbf{M}^{-1}\int_0^1\phi(x)\psi(x)\,dx \tag{17a}$$

$$\dot{\eta}(0)=\mathbf{M}^{-1}\int_0^1\phi(x)\varphi(x)\,dx \tag{17b}$$

Finally, we introduce states $\eta_1\triangleq\eta$ (displacements) and $\eta_2\triangleq\dot{\eta}$ (velocities) to express Eq. (15) in first-order form:

$$\begin{Bmatrix}\dot{\eta}_1\\ \dot{\eta}_2\end{Bmatrix}=\begin{bmatrix}\mathbf{0} & \mathbf{1}\\ -\mathbf{M}^{-1}\mathbf{K} & -\mathbf{M}^{-1}\mathbf{C}\end{bmatrix}\begin{Bmatrix}\eta_1\\ \eta_2\end{Bmatrix}+\begin{Bmatrix}\mathbf{0}\\ \mathbf{M}^{-1}f(t)\,\phi(x_f)-\mathbf{M}^{-1}k\left(\phi(x_k)^{\mathrm{T}}\eta_1(t)\right)^3\phi(x_k)\end{Bmatrix} \tag{18}$$

The final first-order system (Eq. (18)) can be solved numerically using any integration scheme, where the states at time t^i are computed given the states and applied forces at time t^{i-1}. Thus, at the end of time step i, we will know the displacements $\eta_1(t^i)$ and velocities $\eta_2(t^i)$ at time t^i. The continuous displacement and velocity of the beam can then be calculated as $w(x,t^i)=\phi(x)^{\mathrm{T}}\eta_1(t^i)$ and $\partial w(x,t^i)/\partial t^i=\phi(x)^{\mathrm{T}}\eta_2(t^i)$, respectively.

2.1. The Least Absolute Shrinkage and Selection Operator

We wish to find a set of spatial functions $\hat{w}(x,t^i)\triangleq\phi(x)^{\mathrm{T}}\hat{\eta}_1(t^i)$ and $\partial\hat{w}(x,t^i)/\partial t^i\triangleq\phi(x)^{\mathrm{T}}\hat{\eta}_2(t^i)$ such that the following objective functions are minimized:

$$J_1=\min_{\hat{\eta}_1(t^i)}\frac{1}{2}\int_0^1\left(\hat{w}(x,t^i)-w(x,t^i)\right)^2dx \tag{19a}$$

$$J_2=\min_{\hat{\eta}_2(t^i)}\frac{1}{2}\int_0^1\left(\frac{\partial\hat{w}(x,t^i)}{\partial t}-\frac{\partial w(x,t^i)}{\partial t}\right)^2dx \tag{19b}$$

Since the basis functions in the series solution (Eq. (9)) are orthogonal, the objective functions (Eq. (19)) can be simplified as follows:

$$J_k=\min_{\hat{\eta}_k(t^i)}\frac{1}{2}\left\|\hat{\eta}_k(t^i)-\eta_k(t^i)\right\|_2^2,\quad k=1,2 \tag{20}$$

where the squared 2-norm is given by the following:

$$\left\|\hat{\eta}_k(t^i) - \eta_k(t^i)\right\|_2^2 \triangleq \sum_{\ell=1}^{N} \left(\hat{\eta}_{k\ell}(t^i) - \eta_{k\ell}(t^i)\right)^2, \quad k = 1,2 \tag{21}$$

Note that the objective functions (Eq. (20)) simply measure the error between the two solutions, and a minimum is obtained when $\hat{\eta}_k(t^i) = \eta_k(t^i), k = 1,2$. We now impose a constraint and seek sparse $\hat{\eta}_1(t^i)$ and $\hat{\eta}_2(t^i)$ such that objective functions J_1 and J_2 are minimized. The sparsity constraint [7] is introduced by modifying the objective functions (Eq. (20)) as follows:

$$J_k = \min_{\hat{\eta}_k(t^i)} \frac{1}{2} \left\|\hat{\eta}_k(t^i) - \eta_k(t^i)\right\|_2^2 + \lambda \left\|\hat{\eta}_k(t^i)\right\|_1, \quad k = 1,2 \tag{22}$$

where the 1-norm is given by the following:

$$\left\|\hat{\eta}_k(t^i)\right\|_1 \triangleq \sum_{\ell=1}^{N} \left|\hat{\eta}_{k\ell}(t^i)\right|, \quad k = 1,2 \tag{23}$$

Shrinkage parameter $\lambda \geq 0$ controls the amount of sparsity sought in $\hat{\eta}_k(t^i)$, with $\lambda = 0$ corresponding to the true solution. Each constrained objective function (Eq. (22)) represents a convex optimization problem, and has the following closed-form solution [7]:

$$\begin{aligned} \hat{\eta}_k(t^i) &= S_\lambda\left(\eta_k(t^i)\right) \\ &= \max\left\{\mathbf{0}, \left|\eta_k(t^i)\right| - \lambda\right\} \diamond \operatorname{sgn}\left(\eta_k(t^i)\right), \quad k = 1,2 \end{aligned} \tag{24}$$

where S_λ is the shrinkage operator, $\diamond$ represents elementwise vector multiplication, and the signum function $\operatorname{sgn}(\zeta)$ is defined as follows:

$$\operatorname{sgn}(\zeta) = \begin{cases} -1, & \text{if } \zeta < 0 \\ +1, & \text{otherwise} \end{cases} \tag{25}$$

The closed-form solution to the minimization problem (Eq. (24)) may be recognized as *soft thresholding* [13].

In summary, we apply shrinkage operator S_λ to the solution obtained from the numerical integrator $(\eta_k(t^i), k = 1,2)$ to obtain a sparse representation of the solution $(\hat{\eta}_k(t^i))$. The sparse solution provides a concise representation of the system behavior, and does so with minimal computational expense. Also note that the implementation involves simply passing the integrated states through the shrinkage operator at each time step; there is no need to store a matrix of state vector snapshots or employ a computationally expensive decomposition algorithm, as is the case with the POD approach. A potential drawback is that the solutions obtained using the developed approach will deviate from the true solution, propagating absolute error as small amounts of information are lost at each time step. In this application, a considerable amount of sparsity can be introduced into the solution without substantially affecting the simulation results, as we will show.

2.2. Optimal Subset Selection

We also explore the use of an optimal subset selection approach. Since the basis functions in the series solution (Eq. (9)) are orthogonal, the optimal subset selection strategy involves simply retaining the components of the solution whose absolute values are above a specified threshold and zeroing the others [7]:

$$\hat{\eta}_{k\ell}(t^i) = \begin{cases} \eta_{k\ell}(t^i), & \text{if } \left|\eta_{k\ell}(t^i)\right| > \lambda \\ 0, & \text{otherwise} \end{cases}, \quad k = 1,2 \tag{26}$$

which may be recognized as *hard thresholding* [13]. Note that subset selection also involves negligible computational expense, is trivial to implement, and can suffer from the same error propagation issues as the lasso. In contrast to the lasso, however, the retained components of the solution are unaltered—that is, λ is used strictly as a threshold in Eq. (26), not as both a threshold and a scaling parameter as in Eq. (24). As will be shown in the next section, a considerable amount of sparsity can be obtained without introducing substantial errors, even in systems containing strong intermodal coupling.

3. NUMERICAL RESULTS

In this section, we present several numerical test cases to compare the efficacy of the lasso and subset selection approaches. The constrained objective function (Eq. (22)) solved in the lasso approach is minimized to find a sparse solution at each time step of the simulation. Since the sparse solution at time t^i is used to integrate Eq. (18) to time t^{i+1}, the error calculated by the 2-norm in Eq. (22) is a *local* error metric. The errors reported in this section, however, are *absolute* errors, which we calculate by first simulating using each adaptive reduced-order method, and comparing the results to those observed without introducing sparsity. In each test, the same threshold parameter is used for the lasso and subset selection strategies. All numerical results are obtained in Matlab using an explicit fourth-order Runge–Kutta method [2] with an integration time step of $t^{i+1} - t^i = 10^{-4}$. We also fix the number of basis functions at $N = 10$ for each state variable, which we found to be sufficient to achieve convergence, and use damping coefficients $\alpha = \beta = 0.02$ throughout.

3.1. Bilateral Spring

We first consider the system shown in Fig. 1 where the spring is permanently fixed to the beam, thus acting bilaterally. The time response of the beam at $x = x_k$ is shown in Fig. 2(a), where a nonlinear spring of stiffness $k = 1000$ is attached at $x_k = 0.546$ and an external force $f(t) = 10\sin(5\pi t)$ is applied at $x_f = 0.235$; the initial conditions are $\eta_1(0) = \eta_2(0) = \mathbf{0}$. As shown, the classical Galerkin method ($\lambda = 0$) and the two sparse Galerkin methods ($\lambda = 10^{-6}$) produce nearly identical results. Shown in Fig. 2(b) are the number of nonzero terms in the three solutions at each integration time step. All $2N$ terms $\eta_1(t)$ and $\eta_2(t)$ are nonzero throughout the simulation in the classical Galerkin solution, but the lasso and subset selection solutions are both approximately 34% sparse. The absolute error between the classical solution and each sparse solution is defined as follows:

$$e(t) \triangleq \frac{1}{2}\sum_{k=1}^{2} \left\| \hat{\eta}_k(t^i) - \eta_k(t^i) \right\|_2^2 \tag{27}$$

as shown in Fig. 2(c). Note that the error $e(t)$ is more than an order of magnitude lower when using subset selection than when using the lasso, despite these solutions having nearly identical sparsity.

The amount of sparsity is highly dependent on the nature of the time response of the system. To demonstrate, we repeat the above analysis with $k = 5000$, $f(t) = 100\sin(12.6\pi t)$, and initial conditions $\eta_1(0) = \eta_2(0) = \mathbf{0.1}$; all other parameters are the same. In this case, we obtain sparse Galerkin solutions with only 14.3% (lasso) and 13.7% (subset selection) sparsity, as shown in Fig. 3. More sparsity can be obtained by increasing the shrinkage parameter, but not without increasing the error as well. Simulation results using $\lambda = 10^{-5}$ are shown in Fig. 4, where 33.6% (lasso) and 32.2% (subset selection) of the coefficients are zero but the errors have increased substantially. Note that the maximum absolute error increased by one order of magnitude when using the lasso and by two orders of magnitude when using optimal subset selection – although the latter still produced a more accurate solution than the former.

3.2. Unilateral Spring

The system shown in Fig. 1 is now simulated assuming the spring acts only unilaterally, as defined in Eq. (4). We use a spring of stiffness $k = 10^5$ acting at $x_k = 0.55$, an external force $f(t) = 100\sin(12.6\pi t)$ acting at

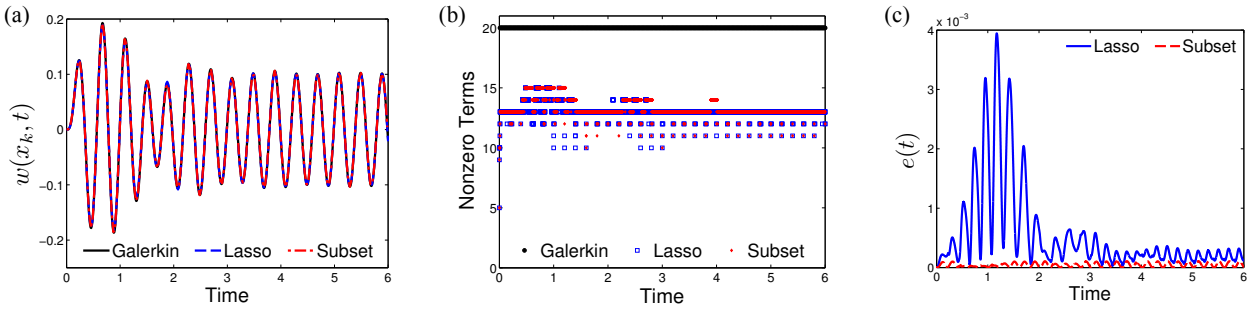

Fig. 2. Simulation results obtained using classical Galerkin ($\lambda = 0$) and sparse Galerkin ($\lambda = 10^{-6}$) methods with a bilateral spring of stiffness $k = 1000$: (a) time response of the beam at the location of the spring, (b) number of nonzero terms in the series solution, and (c) absolute error as a function of time. The lasso and subset selection solutions have sparsities of 34.4% and 33.4%, and maximum absolute errors of 3.9×10^{-3} and 1.1×10^{-4}, respectively.

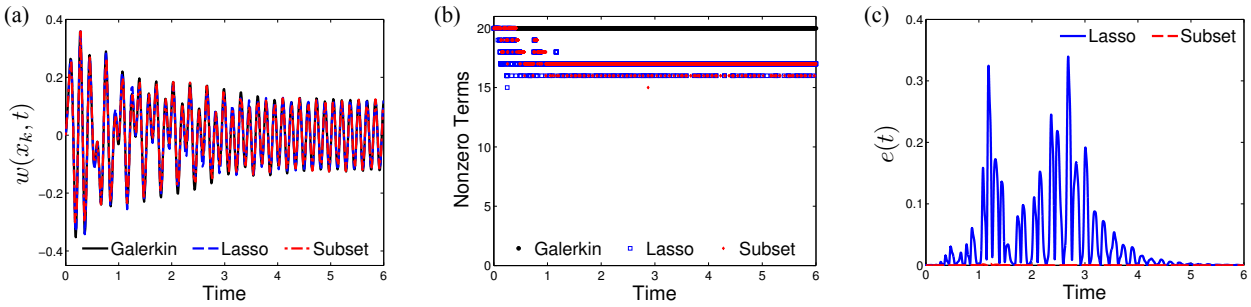

Fig. 3. Simulation results obtained using classical Galerkin ($\lambda = 0$) and sparse Galerkin ($\lambda = 10^{-6}$) methods with a bilateral spring of stiffness $k = 5000$: (a) time response of the beam at the location of the spring, (b) number of nonzero terms in the series solution, and (c) absolute error as a function of time. The lasso and subset selection solutions have sparsities of 14.3% and 13.7%, and maximum absolute errors of 3.4×10^{-1} and 3.4×10^{-3}, respectively.

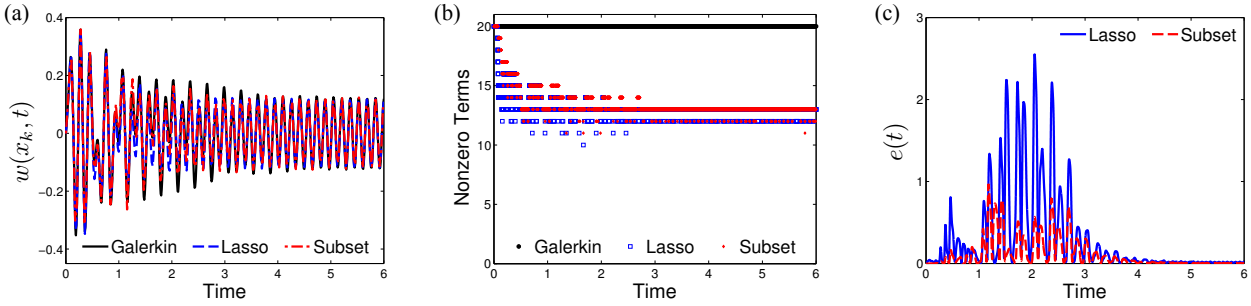

Fig. 4. Simulation results obtained using classical Galerkin ($\lambda = 0$) and sparse Galerkin ($\lambda = 10^{-5}$) methods with a bilateral spring of stiffness $k = 5000$: (a) time response of the beam at the location of the spring, (b) number of nonzero terms in the series solution, and (c) absolute error as a function of time. The lasso and subset selection solutions have sparsities of 33.6% and 32.2%, and maximum absolute errors of 2.6 and 0.96, respectively.

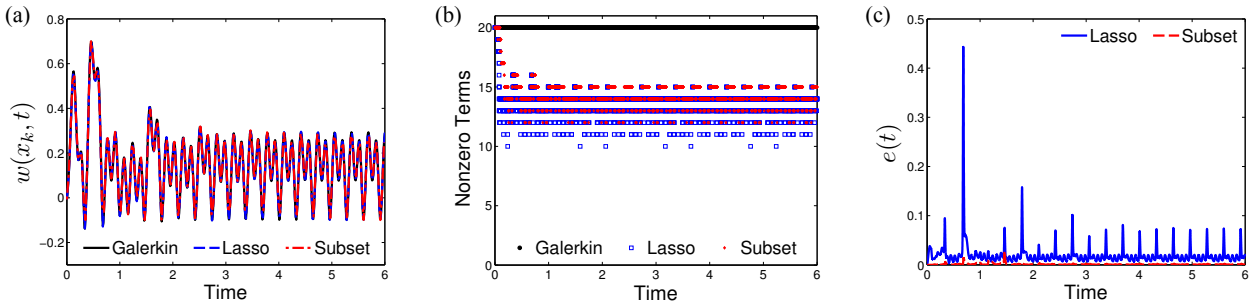

Fig. 5. Simulation results obtained using classical Galerkin ($\lambda = 0$) and sparse Galerkin ($\lambda = 10^{-5}$) methods with a unilateral spring of stiffness $k = 10^5$: (a) time response of the beam at the location of the spring, (b) number of nonzero terms in the series solution, and (c) absolute error as a function of time. The lasso and subset selection solutions have sparsities of 30.9% and 27.1%, and maximum absolute errors of 0.44 and 0.029, respectively.

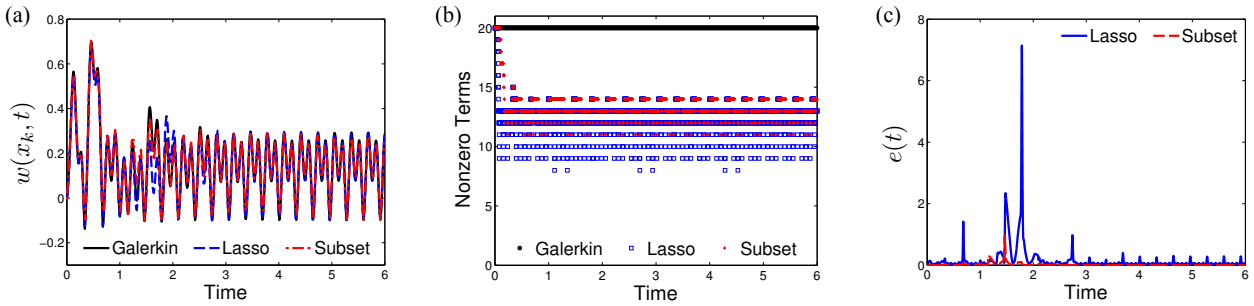

Fig. 6. Simulation results obtained using classical Galerkin ($\lambda = 0$) and sparse Galerkin ($\lambda = 2 \times 10^{-5}$) methods with a unilateral spring of stiffness $k = 10^5$: (a) time response of the beam at the location of the spring, (b) number of nonzero terms in the series solution, and (c) absolute error as a function of time. The lasso and subset selection solutions have sparsities of 35.6% and 32.0%, and maximum absolute errors of 7.1 and 0.96, respectively.

$x_f = 0.33$, and initial conditions $\eta_1(0) = \eta_2(0) = \mathbf{0.1}$. The simulation results are shown in Fig. 5, where we obtain sparsities of 30.9% (lasso) and 27.1% (subset selection) with shrinkage parameter $\lambda = 10^{-5}$. As shown in Fig. 6, doubling λ results in a dramatic increase in absolute error but only a modest increase in sparsity, demonstrating the delicate balance between these objectives.

Finally, Fig. 7 shows the results obtained when the frequency of the forcing function increases linearly with time. In particular, we use $f(t) = 50\sin((3\pi t)t)$ with $\lambda = 10^{-6}$; all other parameters are the same as those used to generate Fig. 6. Even in this highly nonlinear case with a time-varying forcing frequency and strong intermodal coupling, we obtain sparsities of 18.5% (lasso) and 13.4% (subset selection) with reasonable amounts of error. As shown in Fig. 8(a), sparsity increases approximately linearly with exponentially increasing λ, and the solutions generated using the lasso and optimal subset selection approaches have similar sparsity. The maximum error also increases with increasing λ in both cases, as shown in Fig. 8(b), but the lasso generates solutions with errors between one and two orders of magnitude higher than subset selection.

In summary, we obtain sparse solutions at the expense of introducing small amounts of error. The shrinkage operator (Eq. (24)) or optimal subset selection strategy (Eq. (26)) can easily be incorporated into any simulation code that uses spectral methods with orthogonal basis functions to solve partial differential equations. The sparse solutions obtained using the lasso and subset selection can alleviate storage requirements while introducing errors that can be controlled by adjusting a single parameter. Our results indicate that subset selection generates solutions with similar sparsity but substantially lower error than the lasso. Be-

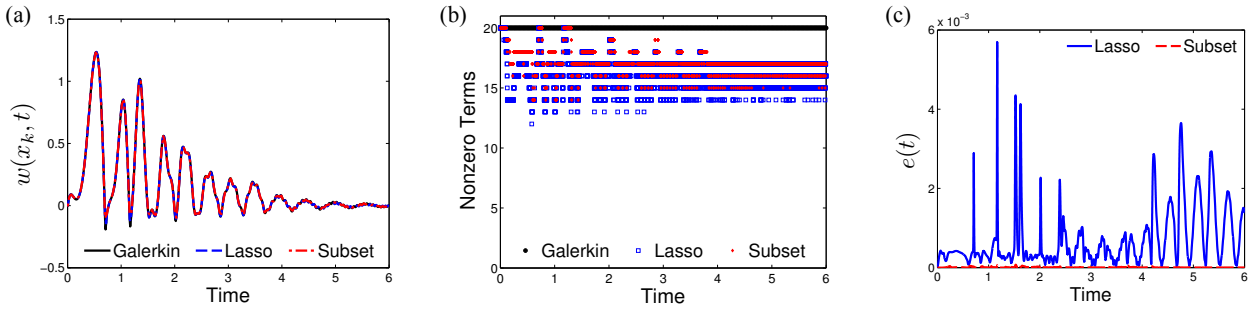

Fig. 7. Simulation results obtained using classical Galerkin ($\lambda = 0$) and sparse Galerkin ($\lambda = 10^{-6}$) methods with a unilateral spring of stiffness $k = 10^5$ and a forcing function with time-varying frequency: (a) time response of the beam at the location of the spring, (b) number of nonzero terms in the series solution, and (c) absolute error as a function of time. The lasso and subset selection solutions have sparsities of 18.5% and 13.4%, and maximum absolute errors of 5.7×10^{-3} and 9.0×10^{-5}, respectively.

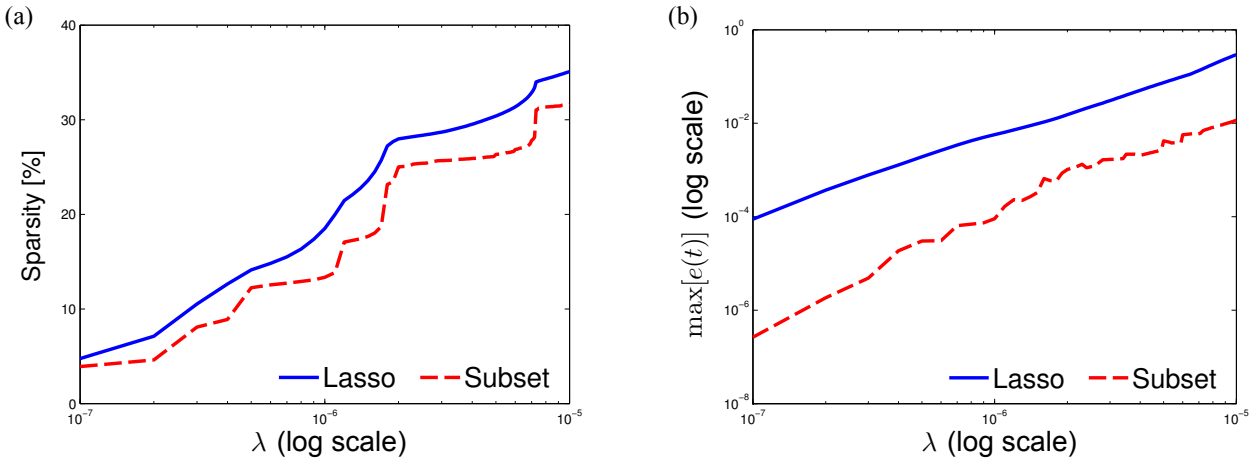

Fig. 8. Simulation results obtained using the lasso and subset selection sparse Galerkin methods with a unilateral spring of stiffness $k = 10^5$ and a forcing function with time-varying frequency: (a) sparsity (linear scale) and (b) maximum error $e(t)$ (logarithmic scale), both as functions of shrinkage parameter λ (logarithmic scale).

cause we always compute all coefficients in the solution, neither sparse strategy offers an advantage in terms of computational speed; however, we discover which modes are active and which modes are insignificant at each time step of the simulation, which is important information. We also note that Schaeffer et al. [6] applied the lasso to PDEs that are first-order in time. We have found that, for PDEs that are second-order in time, the subset selection approach generates better sparse solutions than the lasso.

4. CONCLUSIONS

We have explored two adaptive sparse Galerkin methods for reducing numerical solutions of vibrating continuous structures: the least absolute shrinkage and selection operator (lasso) and the optimal subset selection method. The lasso strategy seeks the most informative subset of coefficients in the series solution by applying a shrinkage operator at each time step of a simulation. The resulting convex optimization problem has a closed-form solution, so can be readily implemented and involves minimal computational expense. The optimal subset selection method also involves negligible computational expense and is trivial to implement.

A vibrating simply supported beam subjected to nonlinear unilateral and bilateral spring forces was used to compare the two methods. In every test case explored, the sparse Galerkin solutions generated using the lasso and optimal subset selection approaches both maintain good agreement with the classical Galerkin solution, but subset selection consistently outperformed the lasso in terms of accuracy. Both approaches can be applied to any vibrating structure whose solution is obtained using spectral methods. This work may be of particular utility for model-predictive controllers, which demand computational efficiency and can tolerate some amount of numerical imprecision.

ACKNOWLEDGEMENTS

C.P.V. wishes to acknowledge Dr. Tamás Kalmár-Nagy for his helpful suggestions on this work. Funding received by C.P.V. from the Department of Science and Technology Inspire Fellowship (grant no. DST/INSPIRE/04/2014/000972) is gratefully acknowledged.

REFERENCES

1. Meirovitch, L., *Dynamics and Control of Structures*, Wiley, New York, 1990.
2. Smith, G.D., *Numerical Solution of Partial Differential Equations: Finite Difference Methods* (3rd ed.), Oxford University Press, New York, 1985.
3. Zienkiewicz, O.C. and Taylor, R.L., *The Finite Element Method, Volume 3: Fluid Dynamics* (5th ed.), McGraw-Hill, London, 2000.
4. Boyd, J.P., *Chebyshev and Fourier Spectral Methods* (2nd ed.), Dover, New York, 2001.
5. Baraniuk, R.G., "Compressive sensing", *IEEE Signal Processing Magazine*, Vol. 24, No. 4, pp. 118–120, 124, 2007.
6. Schaeffer, H., Caflisch, R., Hauck, C.D. and Osher, S., "Sparse dynamics for partial differential equations", *Proceedings of the National Academy of Sciences*, Vol. 110, No. 17, pp. 6634–6639, 2013.
7. Tibshirani, R., "Regression shrinkage and selection via the lasso", *Journal of the Royal Statistical Society. Series B (Methodological)*, Vol. 58, No. 1, pp. 267–288, 1996.
8. Antoulas, A.C. and Sorensen, D.C., "Approximation of large-scale dynamical systems: An overview", *International Journal of Applied Mathematics and Computer Science*, Vol. 11, No. 5, pp. 1093–1121, 2001.
9. Gugercin, S. and Antoulas, A.C., "A survey of model reduction by balanced truncation and some new results", *International Journal of Control*, Vol. 77, No. 8, pp. 748–766, 2004.
10. Kerschen, G., Golinval, J.C., Vakakis, A.F. and Bergman, L.A., "The method of proper orthogonal decomposition for dynamical characterization and order reduction of mechanical systems: An overview", *Nonlinear Dynamics*, Vol. 41, Nos. 1–3, pp. 147–169, 2005.
11. Lall, S., Marsden, J.E. and Glavaški, S., "Empirical model reduction of controlled nonlinear systems", in *Proceedings of the 14th International Federation of Automatic Control World Congress*, H.F. Chen, D.Z. Cheng and J.F. Zhang, eds., pp. 473–478, Beijing, P. R. China, 5–9 July 1999.
12. Vyasarayani, C.P., McPhee, J. and Birkett, S., "Modelling impacts between a continuous system and a rigid obstacle using coefficient of restitution", *ASME Journal of Applied Mechanics*, Vol. 77, No. 2, p. 021008, 2010.
13. Donoho, D.L. and Johnstone, I.M., "Ideal spatial adaptation by wavelet shrinkage", *Biometrika*, Vol. 81, No. 3, pp. 425–455, 1994.